Atmos. Meas. Tech., 2, 159–175, 2009
www.atmos-meas-tech.net/2/159/2009/

Atmospheric Measurement Techniques

Retrieval of temperature, H_2O, O_3, HNO_3, CH_4, N_2O, $ClONO_2$ and ClO from MIPAS reduced resolution nominal mode limb emission measurements

T. von Clarmann[1,*], M. Höpfner[1], S. Kellmann[1], A. Linden[1], S. Chauhan[1], B. Funke[2], U. Grabowski[1], N. Glatthor[1], M. Kiefer[1], T. Schieferdecker[1], G. P. Stiller[1], and S. Versick[1]

[1]Forschungszentrum Karlsruhe, Inst. für Meteorologie und Klimaforschung, Karlsruhe, Germany
[2]Instituto de Astrofísica de Andalucía, CSIC, Spain
[*]temporarily also at: Université de Toulouse, UPS, CNRS, Laboratoire d'Aérologie, 14 avenue Edouard Belin, 31400 Toulouse, France

Received: 18 December 2008 – Published in Atmos. Meas. Tech. Discuss.: 30 January 2009
Revised: 5 May 2009 – Accepted: 5 May 2009 – Published: 12 May 2009

Abstract. Retrievals of temperature, H_2O, O_3, HNO_3, CH_4, N_2O, $ClONO_2$ and ClO from MIPAS reduced spectral resolution nominal mode limb emission measurements outperform retrievals from respective full spectral resolution measurements both in terms of altitude resolution and precision. The estimated precision (including measurement noise and propagation of uncertain parameters randomly varying in the time domain) and altitude resolution are typically 0.5–1.4 K and 2–3.5 km for temperature between 10 and 50 km altitude, and 5–6%, 2–4 km for H_2O below 30 km altitude, 4–5%, 2.5–4.5 km for O_3 between 15 and 40 km altitude, 3–8%, 3–5 km for HNO_3 between 10 and 35 km altitude, 5–8%, 2–3 km for CH_4 between 15 and 35 km altitude, 5–10%, 3 km for N_2O between 15 and 35 km altitude, 8–14%, 2.5–9 km for $ClONO_2$ below 40 km, and larger than 35%, 3–7 km for ClO in the lower stratosphere. As for the full spectral resolution measurements, the reduced spectral resolution nominal mode horizontal sampling (410 km) is coarser than the horizontal smoothing (often below 400 km), depending on species, altitude and number of tangent altitudes actually used for the retrieval. Thus, aliasing might be an issue even in the along-track domain. In order to prevent failure of convergence, it was found to be essential to consider horizontal temperature gradients during the retrieval.

Correspondence to: T. von Clarmann
(thomas.clarmann@imk.fzk.de)

1 Introduction

In March 2004 the MIPAS (Michelson Interferometer for Passive Atmospheric Sounding) (Fischer et al., 2008) on ESA's Envisat research satellite ceased to operate in its full spectral resolution measurement mode. Instead, MIPAS has been operated at reduced spectral but improved spatial resolution since then. While a data product containing vertical profiles of temperature and six trace species was generated by an operational processor (Ridolfi et al., 2000; Raspollini et al., 2006) under ESA responsibility and routinely distributed for the full spectral resolution data, only a limited official reduced spectral resolution data set is available by now (Ceccherini et al., 2008). Instead, research groups which had complemented the operational data product by a scientific data product already when MIPAS was operational at full spectral resolution, have attempted to fill the gap and to provide vertical profiles of temperature and several trace species. One of the data processors used to generate such a scientific data product is the one built and operated in a joint effort by the Institut für Meteorologie und Klimaforschung (IMK) at Forschungszentrum Karlsruhe and the Instituto de Astrofísica de Andalucía (IAA). Recently, the retrieval of temperature, O_3, HNO_3, N_2O and H_2O from reduced spectral resolution so-called "upper troposphere – lower stratosphere #1 (UTLS-1) measurement mode" spectra has been published by Chauhan et al. (2009). In this paper, retrievals of temperature, H_2O, O_3, CH_4, N_2O, HNO_3, $ClONO_2$, and ClO from spectra recorded in the "nominal reduced resolution measurement mode", the measurement mode in which

MIPAS is operated most of its measurement time, are presented and discussed in terms of error analysis and vertical as well as horizontal resolution, and the temporal development of these atmospheric state variables is presented.

2 Measurements

MIPAS performs limb emission measurements from a sun-synchroneous polar orbit at about 800 km altitude. Envisat's equator passing time is about 10 a.m. local time on the southbound leg of the orbit. In the so-called reduced resolution nominal measurement mode, one limb sequence is recorded every 410 km. This horizontal sampling leads to about 100 limb sequences per orbit, depending on time needed for calibration measurements. At polar regions, the nominal tangent altitude spacing is 1.5 km from 6–21 km, 2.0 km from 21–31 km, 3.0 km from 31–46 km and 4 km up to the uppermost tangent altitude which is 70 km (cf. http://www.atm.ox.ac.uk/group/mipas/rrmodes.html). Towards lower latitudes, the entire scan pattern is moved upward by up to 3 km. Since this pattern is denser than the vertical extent of the instantaneous field of view of MIPAS at the tangent point, the atmosphere is oversampled in the vertical dimension. The spectral coverage of MIPAS is 4.15 to 14.6 μm (685–2410 cm^{-1}) at 0.121 cm^{-1} spectral resolution (in terms of full width at half maximum, after application of the Norton Beer "strong" (Norton and Beer, 1976) apodization, corresponding to a maximum optical path difference of 8.2 cm). Data presented in this paper cover the period 27 January 2005 to 8 April 2008, however not at complete temporal coverage. These data are based on 139 824 limb scans recorded during 1626 Envisat orbits.

3 Retrieval

The retrieval strategy applied to the reduced resolution measurements is similar as the one applied to the MIPAS full spectral resolution measurements and has been extensively discussed by von Clarmann et al. (2003). In summary, it is based on constrained inverse modelling of limb radiances.

3.1 Representation of the atmospheric state

The atmosphere is represented on a discrete altitude grid (1-km gridwidth from 4–44 km altitude, 2-km gridwidth from 44–70 km, 5-km gridwidth from 70–120 km, with some additional levels for temperature and H_2O). This grid is a compromise between accuracy and efficiency and has been developed during numerous test retrievals. Depending on the retrieved variable, the formal retrieval quantity is either temperature, volume mixing ratio (vmr) or log(vmr). In case of log(vmr) retrievals particular care is needed when the data are used in a statistical context. Arithmetic averaging will bias the mean values high, if the precision is close to or worse than 100%. Particularly problematic are averages where the expectation value is zero but the true measurements scatter around zero due to measurement noise. In a linear retrieval these noisy values would in tendency cancel out to zero, while arithmetic averaging of results obtained by log-retrievals would, by suppression of negative vmr values but maintaining the positive ones, cause a pronounced bias. Averaging of log-retrievals in the log-domain does not fully remedy the problem because it does not properly account for the natural variability in the sample. The decision for or against the log(vmr) retrieval is made for each species separately under consideration of the gas-specific advantages and drawbacks. Unless explicitly mentioned, the retrievals discussed in this paper are vmr retrievals in the linear domain.

Usually, during analysis of one limb scan the atmosphere is assumed to be horizontally homogeneous with respect to mixing ratios of constituents but horizontally inhomogeneous with respect to temperature. For the latter, a linear horizontal variation was allowed in a range of $\pm$400 km around the nominal geolocation of the limb scan. As already found in the context of the most recent full spectral resolution measurement mode retrievals, the consideration of horizontal temperature gradients generally improves the accuracy of the retrieval, and in many cases it helps to reduce the number of convergence failures. Particularly near the polar vortex boundary many retrievals did not converge when horizontal temperature gradients were ignored.

For reasons extensively discussed in von Clarmann et al. (2003), besides the target quantity, also an additive offset calibration correction per limb scan and per spectral analysis window and a profile of atmospheric background continuum absorption coefficients per spectral analysis window were jointly fitted. While the IMK-IAA MIPAS data processor supports consideration of non-local (non-LTE) thermodynamic equilibrium emissions (Funke et al., 2001, 2005), this is not taken into account for retrieval of species discussed in this paper; instead, the spectral analysis windows were chosen such that non-LTE radiation is best possibly excluded (cf. Sect. 3.4). For the gases discussed in this paper, the same strategy had also been applied to the IMK-IAA full spectral resolution nominal mode retrievals.

3.2 Sequence of operations

The first step of the retrieval chain is determination of the spectral shift of the measurements. Secondly, temperatures and altitude pointing information (i.e. the elevation of the line of sight of the instrument) are jointly retrieved. The following sequence of operations is H_2O, O_3, HNO_3, CH_4 along with N_2O, then $ClONO_2$, and ClO. As a general rule, results of preceding steps are used as input for the subsequent retrieval steps, i.e. the H_2O retrieval uses retrieved temperatures and pointing information, and the subsequent O_3 retrieval uses retrieved H_2O abundances, etc. This approach implies that major contributors to the infrared spectrum are

analyzed first, while analysis of gases with tiny spectral features is postponed until the mixing ratios of the major contributors have been retrieved.

3.3 Regularization

Contrary to the operational MIPAS level-2 processor operated by ESA for analysis of the original full spectral resolution measurements (Ridolfi et al., 2000; Raspollini et al., 2006), which performs maximum likelihood retrievals on a vertical grid defined by the MIPAS tangent altitudes, the IMK-IAA processor performs regularized retrievals on a finer altitude grid (1 km gridwidth in the troposphere up to the middle stratosphere; for details, see Sect. 3.1). Thus, stable solutions can only be obtained by regularization. While other MIPAS processors (Burgess et al., 2004, 2006; Hoffmann et al., 2008) regularize by the maximum a posteriori (also known as "optimal estimation") method (Rodgers, 2000), the IMK-IAA processor uses a smoothing constraint, which operates by weighted minimization of the squared first order finite differences of adjacent profile values, using a Tikhonov (1963) formalism. The intent of this choice is to make the resulting profiles less dependent on the a priori profiles. Details are reported under the respective species. Adjustment of the – in many cases altitude-dependent – strength of the regularization, during a series of test retrievals was driven by the aim to achieve the best possible vertical resolution in the upper troposphere and lower stratosphere at still stable retrievals without unphysical oscillations of the resulting profiles. All trace gases are regularized against an altitude-constant a priori profile. Its actual value is meaningless, since the smoothing regularization applied here affects the shape of the profile only but not the actual values. The altitude-constant choice of the a priori profile avoids artefacts when the altitude of a stratospheric peak or a sharp bend near the tropopause is located at a different altitude in the a priori data compared to the true atmosphere. This approach implies that the resulting profile is, apart from deviations due to measurement, parameter or model errors, a smoothed version of the true profile without bias or further distortion.

The only variables regularized by maximum a posteriori approach are the elevation of the lines of sight (von Clarmann et al., 2003) and the horizontal temperature gradients. The latter (but not the temperatures themselves!) are constrained with a zero order Tikhonov-type regularization towards ECMWF data, which is equivalent to a maximum a posteriori formalism (Rodgers, 2000) with a diagonal ad hoc a priori covariance matrix. The latter was set such that for high altitudes, where ECMWF analysis data are thought to be less reliable, the information on the horizontal temperature gradients is extracted mainly from the measurements, while for lower altitudes, where a single limb scan contains little information on the horizontal temperature distribution but where ECMWF analyses are more reliable, the retrieval is strongly constrained towards the a priori.

3.4 Microwindows

Microwindows are narrow spectral intervals suited for retrieval of temperature or species abundances profiles. Their optimal boundaries are found by minimization of the estimated total error (von Clarmann and Echle, 1998). Starting from a set of automatically generated microwindows (Echle et al., 2000), the microwindow selection used here was modified in order to better remove impact of non-LTE which might have been underestimated in the initial microwindow selection, reduce the impact of further interfering species not yet considered then, and avoid spectral lines whose spectroscopic data prove inconsistent with those of the majority of lines. Details are reported under the respective species. The microwindow selection is listed in Tables 1a–1c.

3.5 Diagnostics

IMK-IAA MIPAS results are characterized by error estimates, as well as vertical and horizontal averaging kernels. The latter two are used to estimate the spatial resolution of the retrievals.

3.5.1 Error analysis

The retrieval error is reported in terms of noise and parameter errors. The former is the mapping of measurement noise onto the retrieval, the latter is the propagation of uncertain parameters (for example the abundance of interfering species) onto the result. The mapping of each of these primary errors onto the retrieved quantity is estimated by application of Gaussian error propagation. The total error in terms of variances is the sum of the error variances of the noise error and all parameter errors. Precision is the total random error including measurement noise and those parameter errors which vary randomly in the time domain. Instrument line shape errors and uncertainties of spectroscopic data are systematic and thus contribute to the total error but not to the precision. Noise is estimated for each individual profile, while the full error analysis is performed for representative profiles only. We assume the following primary errors: 1% for gain calibration uncertainty, 3% uncertainty of the instrument line shape in terms of linear loss of modulation efficiency toward the maximum optical path difference, 150 m elevation pointing uncertainty, 2 K temperature uncertainty (conservatively estimated in order to also account for effects due to suboptimal horizontal representation of the temperature field). Uncertainties of abundances of interfering species, whenever available from a preceding retrieval were accounted for following their dedicated error estimates. When no preceding retrievals were available, and climatological profiles had to be used, uncertainty estimates by Remedios et al. (2007) were used. Noise equivalent spectral radiance typically is 11–19 $\mathrm{nW/(cm^2\,sr\,cm^{-1})}$ in MIPAS band A (695–970 $\mathrm{cm^{-1}}$), relevant to the retrieval of temperature, H_2O,

Table 1a. Microwindows for MIPAS reduced resolution nominal mode retrievals (cm^{-1}).

T+LOS[a]	H_2O	O_3
731.2500–731.8125	795.7500–796.0000	760.6875–761.06250
744.3125–745.5000	808.1875–808.7500	763.5625–764.3125
748.9375–749.8125	825.1250–825.4375	766.8750–767.1875
765.8750–766.5625	827.3750–827.8125	776.1875–776.5000
780.4375–780.6250	1224.7500–1225.2500	777.6875–777.9375
798.1250–798.5000	1239.1250–1239.4375	781.0000–781.7500
810.8125–811.0625	1244.0000–1244.4375	782.5000–782.8750
812.2500–812.5625	1354.6250–1355.0000	787.0000–788.0000
	1362.3125–1362.8125	1029.0000–1031.0000
	1372.0625–1372.5000	1038.0000–1039.0000
	1374.7500–1375.3125	
	1409.5000–1410.1000	

[a] Not all spectral gridpoints are used at each altitude.

Table 1b. Continued.

HNO_3	CH_4+N_2O	$ClONO_2$
862.5000–864.0000	1227.8125–1228.5000	779.5000–781.0000
865.8125–868.0000	1231.1250–1232.5000	
868.2500–871.0000	1234.0000–1235.2500	
871.8125–874.0000	1272.0000–1274.8125	
878.8125–881.3125	1275.4375–1276.7500	
881.6250–883.6250	1290.8125–1292.2500	
	1297.4375–1300.2500	
	1301.6250–1303.1250	

Table 1c. Continued.

ClO[a]
821.0000–823.2500
823.3125–826.2500
826.3125–830.7500
830.8125–835.3750
835.5000–838.5000
838.5625–841.5000
841.5625–846.1875

[a] Not all spectral gridpoints are used at each altitude.

HNO_3, $ClONO_2$ and ClO; 8.5 nW/(cm^2 sr cm^{-1}) in band AB (1020–1170 cm^{-1}), relevant to the retrieval of O_3 and 6 nW/(cm^2 sr cm^{-1}) in MIPAS band B (1215–1500 cm^{-1}), relevant to the retrieval of H_2O, CH_4 and N_2O, all values after apodization. The following uncertainties in spectroscopic data were assumed (based on estimates by J.-M. Flaud, personal communication, 2008): the uncertainties of line intensities and broadening coefficients, respectively are: for CO_2 3 to 5% (at the band head, depending on the vibrational band, and increasing towards higher rotational quantum numbers) and 6%; for H_2O 3–15% and 20%; for O_3 2–30% (the latter value for some hot bands) and 12%; for HNO_3 8–15% and 25%; for CH_4 2–8% and 25%; for N_2O 4–6% (at the band head, depending on the vibrational band, and increasing towards higher rotational quantum numbers) and 7%; and for ClO 15%. The uncertainty of $ClONO_2$ absorption cross-sections is estimated at 5%. The smoothing error (Rodgers, 2000) is not included; we report the spatial resolution instead. The reason for this choice is that the smoothing error depends on the actual variability of the respective state variable, on which for some species no robust knowledge is available.

3.5.2 Vertical averaging kernels

The vertical averaging kernel is the derivative of the retrieved profile with respect to the true profile (Rodgers, 2000). Any deviation from unity of the averaging kernel matrix characterizes the influence of the a priori information used to constrain the retrieval. When a retrieval grid is used which is finer than the altitude sampling of the measurement and no significant altitude information is contained in the spectral line shape, the largest values to be expected for an ideal retrieval where regularization compensates for vertical oversampling only are approximately the quotient of retrieval gridwidth over measurement gridwidth. We use the half-width of the row of the averaging kernel matrix to characterize the vertical resolution of the retrieval at the respective altitude. Due to regularization, the vertical resolution is usually wider than the tangent altitude spacing, and certainly wider than the grid on which the retrieval is performed (Table 2).

3.5.3 Horizontal averaging kernels

Most atmospheric state variables are assumed to vary only with altitude, while during the analysis of one limb scan no horizontal variation of the atmospheric state has been considered. The only exception is temperature, where a linear horizontal variation is allowed to avoid convergence problems at the boundary of the polar vortex. The assumption of local horizontal homogeneity of vmr causes horizontal smoothing, which is characterized by the horizontal averaging kernel (von Clarmann et al., 2008). This method has been extended such that a gain function with regularization term could be used and the retrieval grid could be defined independent of the tangent altitude grid. Consideration of regularization in the altitude domain complicates the assessment of horizontal smoothing, because, contrary to the simpler case of unconstrained maximum likelihood retrievals, there is interaction of horizontal and vertical smoothing. We characterize the horizontal smoothing in a 2-dimensional grid of i altitudes and j latitudes and by the $i \times j$ horizontal averaging kernel matrix $\boldsymbol{A}_{\mathrm{hor}}$. The k-th row of $\boldsymbol{A}_{\mathrm{hor}}$ represents the weights of

Table 2. Vertical resolution for selected altitudes, in terms of full width at half maximum of the row of the profile averaging kernels.

Altitude km	T km	H_2O km	O_3 km	HNO_3 km	CH_4 km	N_2O km	$ClONO_2$ km	ClO km
50.	2.69	6.87	3.53	7.03	3.72	5.79	8.14	18.4
40.	1.93	4.11	2.71	5.96	3.20	3.13	9.13	12.8
30.	2.53	3.56	3.56	3.72	2.96	3.28	3.83	7.49
20.	2.63	2.32	2.42	3.20	1.98	2.47	2.94	3.32
10.	3.42	3.31	2.88	3.40	3.92	3.73	3.24	6.47

all latitudes[1] 1 to j contributing to the result assigned to the altitude k and the nominal latitude of the 1-dimensional profile retrieval. Each element $a_{\mathrm{hor};k,l}$ is calculated from the full two-dimensional $i\times(i\times j)$ averaging kernel matrix $\boldsymbol{A}_{\mathrm{2D}}$ by summation over those elements $a_{\mathrm{2D};k,m}$ of $\boldsymbol{A}_{\mathrm{2D}}$ which represent the lth latitude. The horizontal averaging kernels give a measure of the horizontal smearing characteristics of the MIPAS retrievals. For more quantitative applications like construction of observation operators for data assimilation applications, the use of the full two-dimensional averaging kernels is recommended.

Unless limited by horizontal sampling, the horizontal resolution of the MIPAS retrievals can be estimated by the full width at half maximum of the row of the horizontal averaging kernel matrix (Table 3). The information displacement can be estimated as the horizontal distance of the median of the horizontal averaging kernel and the nominal geolocation of the limb scan. In case of MIPAS, the latter is the geolocation of the tangent point of the measurement at the middle tangent altitude of the limb scan. We use a sign convention that positive displacement is displacement towards the satellite (Table 4).

4 Temperature and line of sight

The retrieval strategy for temperature and elevation of the line of sight (LOS) from CO_2 emissions follows the one applied to MIPAS full resolution spectra (von Clarmann et al., 2003) except for the following upgrades: The retrieval grid has been modified (1-km gridwidth from 4–50 km altitude, 2-km gridwidth from 50–70 km, 2.5-km gridwidth from 70–80 km, 5.0 km gridwidth from 80–110 km, and a 10 km step from 110 to 120 km). Also parameter settings relevant to numerical integration over wavenumber, instrument field of view etc. within the radiative transfer forward model have been re-adjusted in order to obtain an optimal trade-off between accuracy and efficiency. All microwindows used are located in the shortwave wing of the 15 μm CO_2 band system (Table 1a). Some gridpoints within the microwindows which were particularly sensitive to interfering species were discarded, and the selection of microwindows is altitude-dependent, i.e. a particular microwindow is not always used for all tangent altitudes. Compared to the original temperature retrievals published by von Clarmann et al. (2003), microwindows in the 15 μm band system below 700 cm^{-1}, where the spectrum is fairly saturated, and the microwindow in the CO_2 laser band, where non-LTE is a particular issue, have been discarded in favour of further microwindows in the 730–810 cm^{-1} spectral range. The current microwindow selection is not a modification of the old one but has been newly constructed from scratch for the UTLS-1 reduced resolution mode retrievals by Chauhan et al. (2009) and further modified for reduced resolution nominal mode measurements.

ECMWF analysis and MIPAS engineering information is used as a priori information for temperature and line of sight elevation, respectively. Along with the temperature profile, a profile of latitudinal horizontal temperature gradients is retrieved, such that a temperature field is retrieved which varies linearly in the horizontal. This linear variation is confined to $\pm$400 km around the nominal geolocation of the limb scan under analysis. For the horizontal temperature gradients, the ECMWF analysis is used as a priori information, and for regularization the maximum a posteriori approach (Rodgers, 2000) has been chosen.

Further, the climatological CO_2 profiles are trend-corrected. CO_2 ground values are calculated as

$$[\mathrm{CO_2}]=376\,\mathrm{ppmv}+1.9\,\frac{\mathrm{ppmv}}{\mathrm{yr}}\times(\mathrm{year}-2004) \qquad (1)$$

and the vertical profile is scaled by the ratio of the actual ground value and the reference value of the year 2004. The above linear fit of the CO_2 trend is based on the graph of monthly mean carbon dioxide globally averaged over marine sites, as issued in September 2007 by NOAA (Pieter Tans, NOAA/ESRL (www.esrl.noaa.gov/gmd/ccgg/trends)). CO_2 spectroscopic data are taken from the most recent version of the dedicated MIPAS spectroscopy database (Flaud et al., 2006).

The most recent temperature data version is V4o_T_204, where 4o indicates that ESA level 1 spectra version

[1] Instead of "latitudes" this should, for an instrument with its line of sight in the orbit plane, read "along track coordinate"; since the MIPAS orbit is nearly polar, we call this coordinate "latitude" for brevity.

Table 3. Horizontal resolution in terms of full width at half maximum of the row of the horizontal averaging kernels.

Altitude km	T km	H_2O km	O_3 km	HNO_3 km	CH_4 km	N_2O km	$ClONO_2$ km	ClO km
50.	260.	361.	313.	396.	324.	406.	473.	536.
40.	402.	436.	405.	487.	468.	453.	490.	533.
30.	297.	200.	271.	224.	238.	438.	219.	501.
20.	410.	336.	343.	441.	334.	334.	466.	464.
10.	128.	206.	253.	252.	198.	374.	252.	595.

Table 4. Information displacement, calculated as the distance between the median of the row of the horizontal averaging kernel and the nominal geolocation of the MIPAS limb. A positive sign represents displacement towards the satellite. The column "tp" represents the displacement explained by measurement geometry, i.e. the displacement of the tangent point from the nominal geolocation of the limb scan, which is the geolocation of the tangent point of the middle tangent altitude of the limb scan.

Altitude km	tp km	T km	H_2O km	O_3 km	HNO_3 km	CH_4 km	N_2O km	$ClONO_2$ km	ClO km
50.	−65.	−42.	−115.	−104.	−74.	−92.	−69.	−51.	−11.
40.	−42.	−26.	−63.	−62.	−40.	−72.	−55.	−37.	−13.
30.	−14.	336.	−1.	−18.	−21.	34.	421.	−21.	14.
20.	34.	262.	45.	48.	49.	46.	95.	44.	45.
10.	92.	156.	−112.	73.	143.	126.	169.	135.	126.

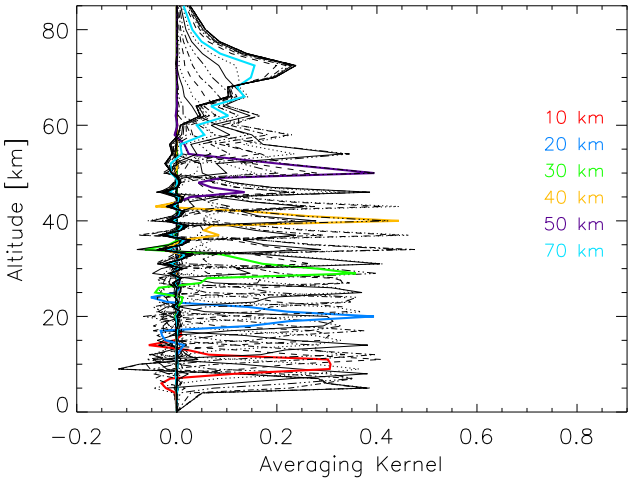

Fig. 1. Rows of the averaging kernel matrix for temperature, evaluated for the limb scan recorded at 61° N, 124° W on 27 January 2005. Selected altitudes are highlighted by colours.

IPF/4.65-IPF/4.67 are used, 2xx indicates that it is reduced spectral resolution nominal mode data, and 4 is the specific data version for temperature.

The original full-resolution data were validated by Wang et al. (2005). The MIPAS UTLS-1 retrievals have been compared to Microwave Limb Sounder (MLS) data by Chauhan et al. (2009); the retrieval setup of the UTLS-1 and the reduced resolution nominal mode retrievals differ only in a few details (see below), and the differences of the datasets are the wider altitude coverage of the nominal measurements and the finer horizontal sampling of the UTLS-1 measurements.

Table 5 summarizes the temperature error analysis evaluated for a limb scan recorded at 61° N, 124° W on 06:26:19 UTC (22:10:19 local mean time, nighttime conditions) on 27 January 2005 during Envisat orbit 30721. The dominating error source below 30 km altitude is the gain calibration error, while at higher altitudes instrument line shape (ILS) uncertainties are the largest error component. Further important error sources are uncertainties in the assumed abundances of N_2O_5 and O_3 as well as measurement noise. Spectroscopic data account for an additional estimated uncertainty of 0.1–0.6 K. Compared to MIPAS full spectral resolution temperature retrievals, the measurement noise is slightly reduced, while the other error components are of comparable size.

Figure 1 shows the vertical averaging kernels of this particular retrieval. The altitude resolution is between 2 and 3.5 km between 10 and 45 km altitude (Table 2), which is slightly better than that of MIPAS full spectral resolution measurements, for which the altitude resolution of temperature was estimated at 4 km in this altitude range.

The horizontal smoothing varies between about 128 km (at 10 km altitude, Table 3) and 499 km at 13 km altitude, with values around 300 km throughout wide parts of the

Table 5. Temperature retrieval error budget.

Height km	Noise K	Gain K	N_2O_5 K	O_3 K	Precision K	ILS K	Spectroscopy K	Total error K
50	0.8	0.4	1.1	0.2	1.4	1.4	0.5	2.1
45	0.4	0.4	0.9	0.1	1.1	1.0	0.1	1.5
40	0.4	0.4	0.6	0.1	0.8	0.8	0.4	1.2
35	0.3	0.4	0.1	0.0	0.5	0.4	0.4	0.8
30	0.3	0.4	0.0	0.2	0.5	0.2	0.1	0.5
25	0.3	0.4	0.1	0.4	0.6	0.4	0.6	0.9
20	0.3	0.3	0.0	0.3	0.6	0.4	0.2	0.8
15	0.2	0.3	0.0	0.3	0.5	0.7	0.1	0.9
10	0.2	0.4	0.0	0.2	0.5	0.2	0.1	0.5

atmosphere, which is less than the horizontal sampling of MIPAS reduced resolution nominal mode measurements. According to the sampling theorem, all periodic atmospheric structures of wavelengths shorter than 2×410 km are prone to aliasing, unless the limited horizontal resolution of the measurement filters out these short-wavenumber components. For the actual horizontal resolution of the MIPAS retrievals, however, the horizontal smearing is not sufficient to act as anti-aliasing filter. The risk of aliasing has been reported for full-resolution MIPAS retrievals by von Clarmann et al. (2008). For reduced resolution nominal mode measurements, however, this risk is not as large as with the measurements taken in the reduced resolution UTLS-1 measurement mode (Chauhan et al., 2009), where the horizontal smoothing width is at some altitudes smaller than the horizontal sampling by a factor of about three. The aliasing problem is of general nature and does affect retrievals of all state variables of the atmosphere whose horizontal averaging kernels are narrow enough. It is not limited to temperature retrievals.

At 10 km the information displacement of the reduced resolution nominal mode measurements is larger than the horizontal smoothing width (Table 4), which means that the measurement contains little information about the temperature at the nominal geolocation of the measurement but on geolocations closer to the sub-satellite point.

Figure 2 shows, as an example, the inner tropical (averaged over 10.0° S to 10.0° N) temperature from February 2005 to April 2008 as a function of altitude. Cold tropopause temperatures from January to May occur in each year.

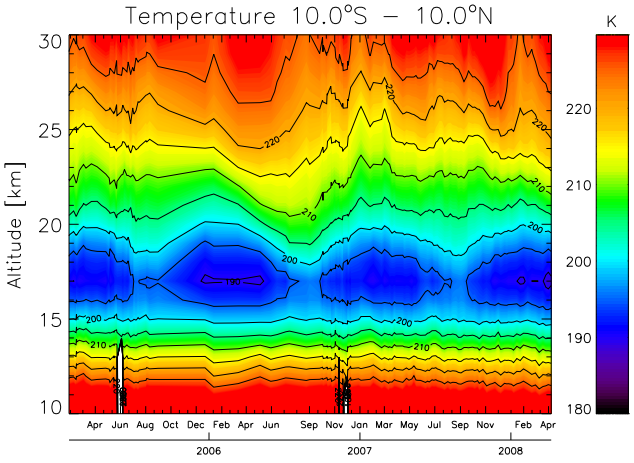

Fig. 2. Temporal development of temperature as a function of altitude in the inner tropics (averaged from 10° S to 10° N).

5 H_2O

Since the work of Milz et al. (2005) (versions V1_H2O_01 to V2_H2O_5) the following retrieval upgrades have been made for the most recent version V4o_H2O_203 (same version coding as for temperature): Microwindows in the central region of the 6.3 μm band of H_2O, where the atmosphere is optically rather thick, and in the region of the CO_2 laser band, where non-LTE of CO_2 turned out to be a problem have been discarded (Table 1a). Instead, some microwindows have been added in the 1360–1375 cm^{-1} spectral region. In addition, the microwindow boundaries have been adjusted to the spectral resolution and sampling of the reduced resolution measurements. Measurements in MIPAS band C (1570–1750 cm^{-1}) covering the 6.3 μm-band of H_2O have finally been discarded because of problems with non-LTE and interference by NO_2. Discard of these transitions unfortunately leads to reduced sensitivity of the H_2O retrieval above 50 km, which is why these transitions were considered in some previous data versions. H_2O spectroscopic data are taken from the most recent version of the dedicated MIPAS spectroscopy database (Flaud et al., 2006). As for all other gas retrievals, horizontal temperature gradients are taken into account.

While for most other trace gases the vmr is retrieved directly, for H_2O we retrieve log(vmr). This allows for an altitude-, latitude- and season-independent a priori profile

Table 6. H_2O retrieval error budget.

Height km	Noise ppbv (%)	Pointing ppbv (%)	Gain ppbv (%)	T ppbv (%)	Precision ppbv (%)	ILS ppbv (%)	Spectroscopy ppbv (%)	Total error ppbv (%)
50	840.0 (14.1)	140.0 (2.4)	330.0 (5.6)	68.0 (1.1)	915.8 (15.4)	50.0 (0.8)	330.0 (5.6)	974.7 (16.4)
40	470.0 (6.7)	190.0 (2.7)	22.0 (0.3)	160.0 (2.3)	532.1 (7.5)	180.0 (2.6)	710.0 (10.1)	905.3 (12.8)
35	340.0 (5.5)	160.0 (2.6)	24.0 (0.4)	150.0 (2.4)	405.3 (6.6)	130.0 (2.1)	970.0 (15.7)	1059.3 (17.1)
30	250.0 (4.5)	110.0 (2.0)	130.0 (2.3)	100.0 (1.8)	318.6 (5.7)	150.0 (2.7)	950.0 (17.0)	1013.2 (18.2)
25	180.0 (4.2)	160.0 (3.7)	67.0 (1.6)	92.0 (2.1)	266.4 (6.2)	68.0 (1.6)	770.0 (18.0)	817.6 (19.1)
20	150.0 (3.4)	130.0 (2.9)	150.0 (3.4)	77.0 (1.7)	260.4 (5.8)	87.0 (1.9)	740.0 (16.6)	789.3 (17.7)
15	150.0 (3.1)	120.0 (2.5)	110.0 (2.3)	100.0 (2.1)	242.9 (5.1)	47.0 (1.0)	720.0 (15.0)	761.3 (15.8)
10	130.0 (3.2)	64.0 (1.6)	140.0 (3.4)	25.0 (0.6)	203.0 (4.9)	59.0 (1.4)	270.0 (6.6)	342.9 (8.3)

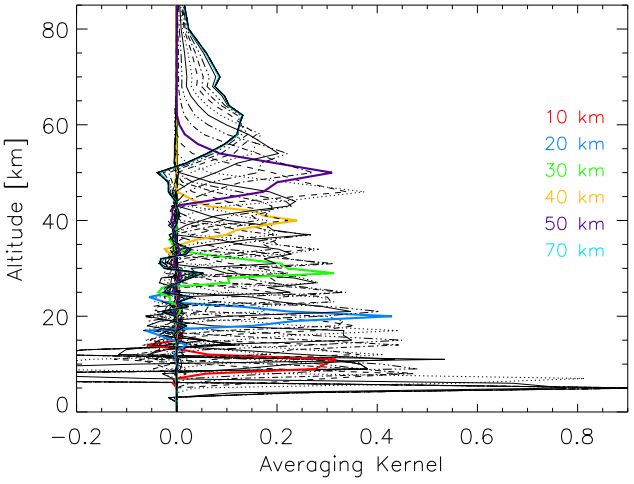

Fig. 3. Rows of the averaging kernel matrix for H_2O. For details, see Fig. 1.

and regularization strength although the variability of water vapour is extremely large particularly in the upper troposphere. On the negative side, the averaging kernels refer to log(vmr) and thus are not as easy to interpret, and averages of H_2O values may be biased high, particularly if in a dry atmospheric region the spread is caused primarily by the propagation of measurement errors rather than natural variability. Further, the H_2O profile is sampled on a 10-km grid only above 80 km.

Beyond these changes in the H_2O retrieval setup, certainly all changes in the setup of the temperature and line of sight retrieval also affect the subsequent H_2O retrieval and thus have to be considered also in the H_2O data version management. This version-interdependence does not only apply to H_2O but to all retrievals of species which use results of preceding retrievals.

The total retrieval error, evaluated for the limb scan recorded at 61° N, 124° W on 27 January 2005, varies between 0.3 and 1.1 ppmv (Table 6) and is dominated by uncertainties of spectroscopic parameters which contribute to the systematic error, while the precision is much better, except for the stratopause region where the error budget is dominated by measurement noise.

The altitude resolution as inferred from the rows of the vertical averaging kernels (Fig. 3) varies from about 2.3–3.5 km at the lower stratosphere and about 3–4 km at 30 km, and coarser above (Table 2). Particularly at lower altitudes, the altitude resolution of the reduced spectral resolution nominal measurements is better than that of the full resolution measurements, which varies between 3 and 4 km at altitudes between 10 and 40 km for V3o_H2O_13, but coarser than the MIPAS reduced resolution UTLS-1 mode results presented by Chauhan et al. (2009).

The horizontal smoothing varies between about 100 km and 500 km, depending on altitude (Table 3) and is generally better than that of the latest full spectral resolution retrievals (Milz et al., 2009). At most altitudes the horizontal resolution is limited by sampling rather than smoothing, i.e. the atmosphere is undersampled in the horizontal. At all altitudes except the lowest, the information displacement (Table 4) is dominated by the displacement of the actual tangent points of the limb scan with respect to the nominal geolocation of the limb scan. As discussed in von Clarmann et al. (2008), opacity shifts the source region of information towards the satellite at lower altitudes, while a displacement in the opposite direction at higher altitudes is explained by better sampling of the atmosphere behind the tangent point. The erratic negative value at 10 km does not describe the source of information well because the horizontal averaging kernel is quite an irregular distribution with considerable negative values near the nominal geolocation. Thus, it is not easily characterized by its median. The centroid of information, e.g., is +199 km at this altitude.

The MIPAS full spectral resolution retrievals, versions up to V3o_H2O_13 (Milz et al., 2009) have been validated against numerous independent measurements and the reduced resolution UTLS-1 retrievals were compared to MLS by Chauhan et al. (2009). However, the V3o_H2O_13 full

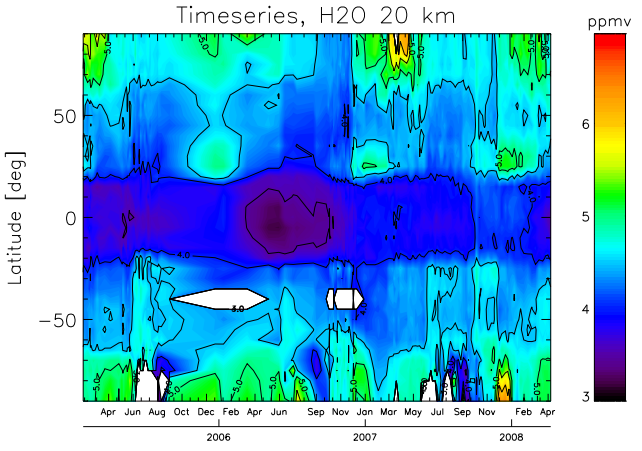

Fig. 4. Temporal development of H_2O as a function of latitude at 20 km altitude. White areas in midlatitudes are data gaps due to calibration measurements. White areas in high southern latitudes are data gaps due to polar stratospheric clouds (PSC).

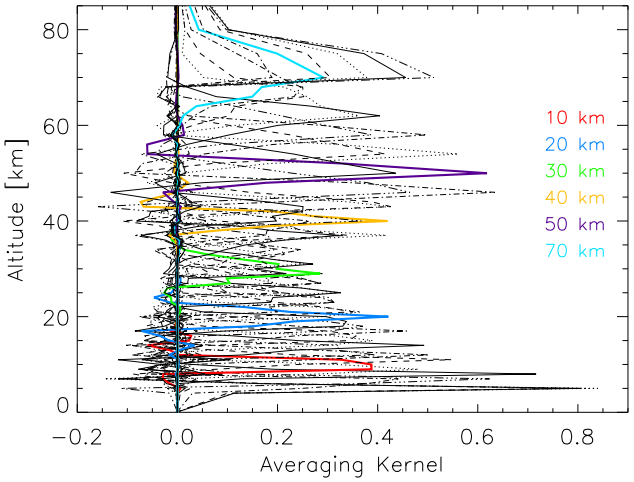

Fig. 5. Rows of the averaging kernel matrix for O_3. For details, see Fig. 1.

spectral resolution microwindows still include transitions in the 6.3 μm region which have been discarded for the reduced spectral resolution analysis. This suggests that a potential bias due to non-local thermodynamic equilibrium emission should be reduced in the reduced resolution nominal mode data set presented here.

Figure 4 shows the latitudinal water vapour distribution at 20 km altitude from February 2005 to April 2008. Most prominent features are dehydration events in Southern polar spring, humid midlatitude winters and dry tropical summers, in particular summer 2006, at this altitude.

6 O_3

Ozone retrievals based on MIPAS full resolution spectra have been extensively studied by Glatthor et al. (2006) and validated by Steck et al. (2007). Since then, the following changes in retrieval strategy have been made: The microwindow selection (Table 1a) has been newly performed from scratch, under consideration of the reduced spectral resolution and modified measurement scenario. While the spectral regions where suitable lines are found remain the same, different ozone transitions have been chosen. As for the MIPAS full spectral resolution retrievals, O_3 spectroscopic data are taken from the most recent version of the dedicated MIPAS spectroscopy database (Flaud et al., 2006). Except for the eight highest altitudes, the strength of the regularization has been chosen independent of altitude.

Also for ozone version V4o_O3_202, the total error budget, evaluated for the limb scan recorded at 61° N, 124° W on 27 January 2005, is dominated by uncertainties of spectroscopic parameters, which account for a relative error of more than 10% at most altitudes. The precision varies between about 50 and 275 ppbv and is limited by gain calibration uncertainties (Table 7).

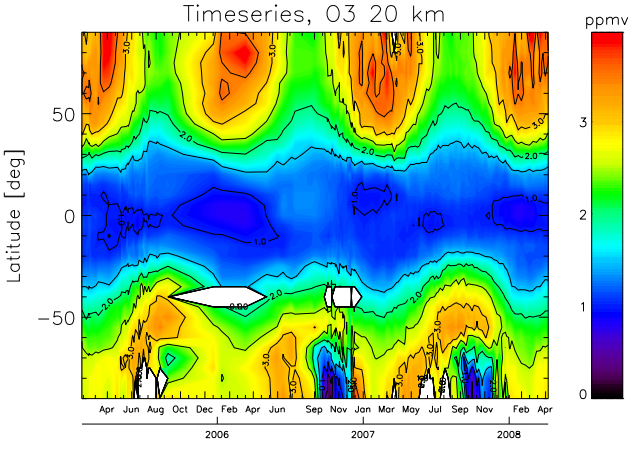

Fig. 6. Temporal development of O_3 as a function of latitude at 20 km altitude. White areas in southern midlatitudes are due to data gaps caused by regular calibration measurements, while white areas at high southern latitudes are data gaps due to polar stratospheric clouds (PSC).

The altitude resolution as inferred from the rows of the vertical averaging kernels (Fig. 5) is about 2.5–3.5 km (Table 2), and is slightly better than that of the latest full spectral resolution retrievals (3.5–5 km between 10 and 40 km altitude for version V3o_O3_9). The horizontal smoothing varies between about 250 km and 400 km and is smaller than the horizontal sampling width of 410 km (Table 3). The horizontal information displacement (Table 4) follows roughly the tangent point displacement, with the usual positive and negative deviations due to opacity and sampling.

Figure 6 shows the latitudinal ozone distribution at 20 km altitude from February 2005 to April 2008. The annual cycle

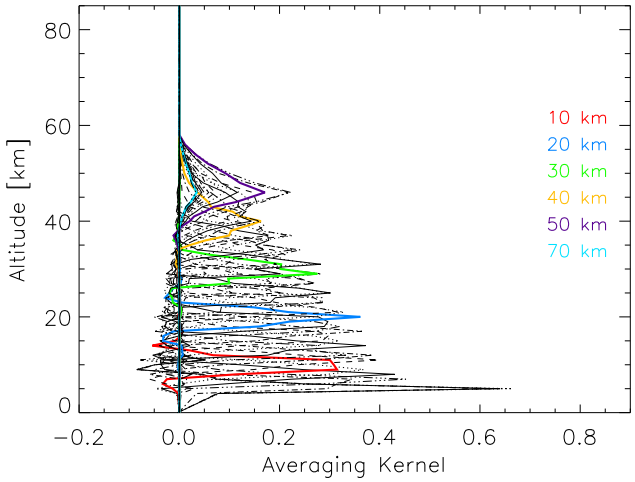

Fig. 7. Rows of the averaging kernel matrix for HNO_3. For details, see Fig. 1.

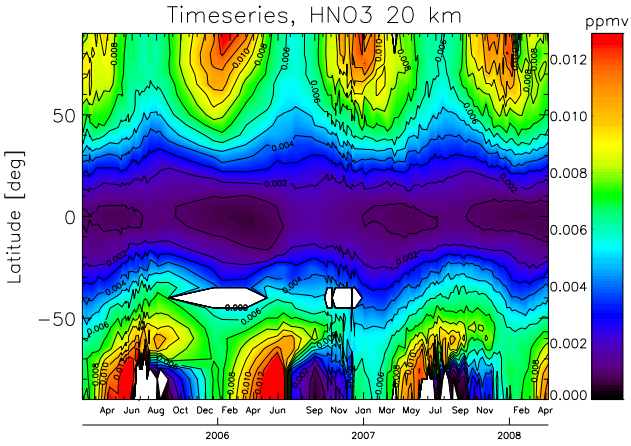

Fig. 8. Temporal development of HNO_3 as a function of latitude at 20 km altitude. White areas in southern midlatitudes are due to data gaps caused by regular calibration measurements, while white areas at high southern latitudes are data gaps due to polar stratospheric clouds (PSC).

is clearly visible. The ozone holes in Southern polar springs 2006 and 2007 are quite prominent, while in 2005 ozone depletion is less pronounced.

7 HNO_3

The reduced resolution nominal mode HNO_3 retrievals version V4o_HNO3_201 are based on full spectral resolution retrievals as published by Mengistu Tsidu et al. (2005), who already used altitude dependent regularization strength (Steck and von Clarmann, 2001; Steck, 2002). Since then, the regularization strength, while still altitude-dependent, has been modified and the microwindows have been adjusted to the spectral sampling of the reduced resolution measurements (Table 1b). However, the same spectral transitions are used as Mengistu Tsidu et al. (2005) used for full spectral resolution measurements. Thus, the lessons learned from the validation of the full spectral resolution HNO_3 retrievals by Wang et al. (2007) should be applicable also to the V4o_HNO3_201 data. HNO_3 spectroscopic data are taken from the dedicated MIPAS spectroscopy database (Flaud et al., 2006). The HNO_3 total retrieval error, evaluated for the limb scan recorded at 61° N, 124° W on 27 January 2005, varies between 4.4 and 17.2% and is noise-dominated below 15 km and above 35 km. In the middle stratosphere the precision is excellent (2.4 to 4.9%) and spectroscopic uncertainties are the major contributor to the total error (Table 8).

The altitude resolution as inferred from the rows of the vertical averaging kernels (Fig. 7) is better than 3.5 km in the lower stratosphere and degrades with altitude towards 6 km at 40 km altitude (Table 2). It is better than that of the latest full spectral resolution retrievals, V3o_HNO3_9 at altitudes below 25 km (on average 4 km) but similar above. The horizontal smoothing width varies between about 250 to 500 km (Table 3) and the horizontal information displacement behaves as expected (Table 4).

Figure 8 shows the latitudinal HNO_3 distribution at 20 km altitude from February 2005 to April 2008. The annual cycle is clearly visible. Denitrification is visible in all Southern polar winters and in northern polar winter 2007/2008.

8 CH_4 and N_2O

As for the full spectral resolution retrievals, also V4o_CH4_201 and V4o_N2O_201 versions of CH_4 and N_2O are retrieved jointly in order to minimize mutual error propagation. In the boundary region of the polar vortex severe convergence problems were encountered before horizontal temperature gradients were considered, and convergence is significantly helped by consideration of these. As for the MIPAS full spectral resolution retrievals (Glatthor et al., 2005), microwindows in the 1220–1305 cm^{-1} spectral regions are used (Table 1b). For some transitions, only the boundaries of the original full spectral resolution microwindows were adjusted, others were exchanged. The goal of these microwindow changes was to reduce the known high bias of CH_4 but this was only partly successful. N_2O spectroscopic data are taken from the HITRAN2K database, while for CH_4 the HITRAN update of 2002 was used (Rothman et al., 2003).

The estimated total retrieval error of CH_4, evaluated for the limb scan recorded at 61° N, 124° W on 27 January 2005, varies between 13 and 34%, and uncertainties in spectroscopic data are the dominating error source (Table 9). The estimated precision is in the order of 5 to 8%, and degrading to 14% towards the stratopause. For N_2O the total retrieval error varies between 8 and 16% in major parts of the

Table 7. O_3 retrieval error budget.

Height km	Noise ppbv (%)	Pointing ppbv (%)	Gain ppbv (%)	T ppbv (%)	Precision ppbv (%)	ILS ppbv (%)	Spectroscopy ppbv (%)	Total error ppbv (%)
50	75.0 (2.1)	180.0 (5.1)	25.0 (0.7)	76.0 (2.1)	210.8 (5.9)	2.5 (0.1)	230.0 (6.5)	312.0 (8.8)
40	50.0 (0.9)	210.0 (3.6)	120.0 (2.1)	130.0 (2.2)	279.1 (4.8)	0.3 (0.0)	650.0 (11.1)	707.4 (12.1)
35	73.0 (1.3)	170.0 (3.1)	95.0 (1.7)	78.0 (1.4)	222.1 (4.0)	85.0 (1.5)	620.0 (11.2)	664.1 (12.0)
30	67.0 (1.1)	200.0 (3.3)	130.0 (2.2)	67.0 (1.1)	256.7 (4.3)	170.0 (2.8)	720.0 (12.1)	783.1 (13.1)
25	60.0 (1.0)	220.0 (3.7)	130.0 (2.2)	85.0 (1.4)	275.9 (4.7)	130.0 (2.2)	700.0 (11.9)	763.6 (12.9)
20	46.0 (1.3)	51.0 (1.4)	120.0 (3.3)	22.0 (0.6)	140.0 (3.8)	89.0 (2.4)	410.0 (11.2)	442.3 (12.1)
15	33.0 (1.9)	1.7 (0.1)	62.0 (3.6)	9.8 (0.6)	70.9 (4.1)	28.0 (1.6)	150.0 (8.6)	168.3 (9.6)
10	28.0 (7.0)	38.0 (9.5)	13.0 (3.2)	13.0 (3.2)	50.7 (12.6)	22.0 (5.5)	40.0 (10.0)	68.2 (17.0)

Table 8. HNO_3 retrieval error budget.

Height km	Noise pptv (%)	Pointing pptv (%)	Gain pptv (%)	T pptv (%)	Precision pptv (%)	ILS pptv (%)	Spectroscopy pptv (%)	Total error pptv (%)
40	88.0 (15.6)	36.0 (6.4)	3.9 (0.7)	2.5 (0.4)	95.2 (16.8)	7.4 (1.3)	17.0 (3.0)	97.0 (17.2)
35	79.0 (3.8)	140.0 (6.7)	29.0 (1.4)	22.0 (1.1)	164.8 (7.9)	24.0 (1.2)	170.0 (8.2)	238.0 (11.4)
30	67.0 (0.9)	330.0 (4.6)	94.0 (1.3)	65.0 (0.9)	355.6 (4.9)	79.0 (1.1)	640.0 (8.9)	736.4 (10.2)
25	62.0 (0.6)	160.0 (1.5)	150.0 (1.4)	93.0 (0.9)	246.2 (2.4)	130.0 (1.3)	780.0 (7.5)	828.2 (8.0)
20	54.0 (0.7)	150.0 (1.9)	170.0 (2.1)	57.0 (0.7)	239.9 (3.0)	110.0 (1.4)	440.0 (5.5)	513.1 (6.4)
15	50.0 (0.8)	48.0 (0.8)	160.0 (2.7)	45.0 (0.8)	180.1 (3.0)	80.0 (1.3)	170.0 (2.8)	260.2 (4.4)
10	40.0 (2.4)	68.0 (4.2)	45.0 (2.8)	14.0 (0.9)	91.9 (5.6)	12.0 (0.7)	31.0 (1.9)	97.7 (6.0)

stratosphere and reaches 30.5% at the stratopause. For N_2O the dominating error source at altitudes up to 35 km is uncertainties in spectroscopic data, while above measurement noise is the leading source of error (Table 10).

Both the full and the reduced spectral resolution CH_4 and N_2O retrievals with the IMK-IAA processor are known to be biased high, particularly in the lowermost stratosphere (Glatthor et al., 2005). This bias, which, however, is within the error margins associated with uncertainties in spectroscopc data, is smaller in the reduced resolution data compared to the full spectral resolution retrievals.

The altitude resolution as inferred from the rows of the vertical averaging kernels (Figs. 9 and 11) is around 2–3 km in the altitude region between 15 and 35 km for both species. At the tropopause region and in the upper stratosphere it is 4 km or even worse (Table 2). At these altitudes the altitude resolution of full spectral resolution retrievals V3o_N2O_11 and V3o_CH4_11 is 4 km and 6 km, respectively. The horizontal smoothing varies between about 140 and 470 km for CH_4 and between 190 and 540 km for N_2O (Table 3). For CH_4, the horizontal displacement behaves roughly as expected, while for N_2O there is an erratic value (421 km) at 30 km altitude (Table 4). In this case, also the centroid of information is quite large (246 km). The horizontal averaging kernel is bimodal, with a broad maximum at +450 km displacement and secondary maximum around zero displacement. While the

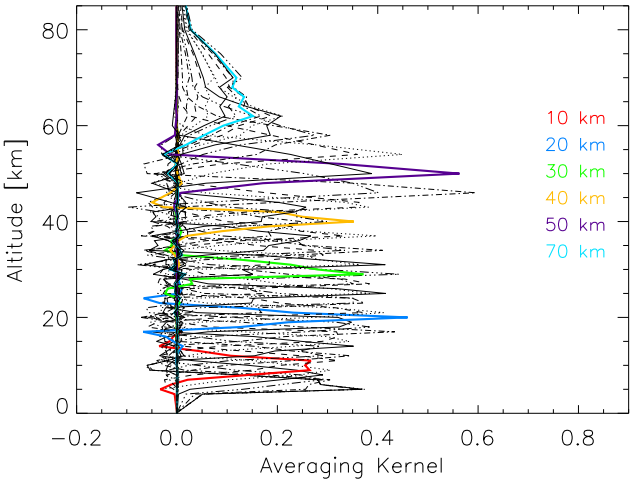

Fig. 9. Rows of the averaging kernel matrix for CH_4. For details, see Fig. 1.

latter are associated with N_2O emissions near the tangent point, the largely displaced information is associated with tropospheric tangent altitudes.

Figure 10 shows the Southern polar (averaged over 60.0° S to 90.0° S) CH_4 mixing ratios from February 2005 to April 2008 as a function of altitude. CH_4-poor mesospheric air

Table 9. CH_4 retrieval error budget.

Height km	Noise ppbv (%)	Pointing ppbv (%)	Gain ppbv (%)	T ppbv (%)	Precision ppbv (%)	ILS ppbv (%)	Spectroscopy ppbv (%)	Total error ppbv (%)
50	31.0 (12.5)	12.0 (4.8)	5.0 (2.0)	8.9 (3.6)	34.8 (14.0)	7.8 (3.1)	5.9 (2.4)	36.1 (14.6)
40	33.0 (7.0)	17.0 (3.6)	13.0 (2.8)	16.0 (3.4)	42.5 (9.0)	19.0 (4.0)	50.0 (10.6)	68.3 (14.5)
35	29.0 (4.8)	26.0 (4.3)	18.0 (3.0)	21.0 (3.4)	47.8 (7.8)	26.0 (4.3)	130.0 (21.3)	140.9 (23.1)
30	44.0 (5.2)	21.0 (2.5)	4.9 (0.6)	15.0 (1.8)	51.2 (6.1)	49.0 (5.8)	120.0 (14.2)	139.4 (16.6)
25	47.0 (3.5)	75.0 (5.6)	1.2 (0.1)	24.0 (1.8)	91.7 (6.9)	40.0 (3.0)	300.0 (22.6)	316.2 (23.8)
20	49.0 (3.8)	50.0 (3.9)	2.8 (0.2)	12.0 (0.9)	71.1 (5.6)	6.4 (0.5)	270.0 (21.1)	279.3 (21.8)
15	65.0 (3.4)	37.0 (1.9)	6.4 (0.3)	65.0 (3.4)	99.3 (5.2)	7.6 (0.4)	230.0 (12.0)	250.6 (13.1)
10	72.0 (4.0)	60.0 (3.4)	4.1 (0.2)	59.0 (3.3)	110.8 (6.2)	20.0 (1.1)	200.0 (11.2)	229.5 (12.9)

Table 10. N_2O retrieval error budget.

Height km	Noise ppbv (%)	Pointing ppbv (%)	Gain ppbv (%)	T ppbv (%)	Precision ppbv (%)	ILS ppbv (%)	Spectroscopy ppbv (%)	Total error ppbv (%)
50	0.7 (30.1)	0.1 (2.3)	0.0 (0.3)	0.0 (1.1)	0.7 (30.2)	0.0 (0.9)	0.1 (4.0)	0.7 (30.5)
40	0.9 (9.8)	0.4 (4.2)	0.1 (1.6)	0.2 (2.4)	1.0 (11.1)	0.2 (2.6)	0.5 (6.1)	1.1 (12.9)
35	1.3 (6.0)	1.5 (7.0)	0.6 (2.8)	0.8 (3.7)	2.2 (10.3)	1.0 (4.6)	2.4 (11.1)	3.4 (15.9)
30	2.8 (4.8)	2.6 (4.4)	0.0 (0.1)	0.8 (1.3)	3.9 (6.7)	1.8 (3.1)	5.9 (10.1)	7.3 (12.5)
25	4.5 (2.8)	12.0 (7.5)	0.1 (0.1)	3.7 (2.3)	13.3 (8.3)	3.4 (2.1)	19.0 (11.9)	23.5 (14.7)
20	4.8 (2.4)	7.3 (3.7)	0.6 (0.3)	1.1 (0.6)	8.8 (4.5)	0.0 (0.0)	22.0 (11.1)	23.7 (12.0)
15	6.3 (2.1)	7.5 (2.5)	0.6 (0.2)	9.8 (3.3)	13.9 (4.7)	0.5 (0.2)	25.0 (8.4)	28.6 (9.6)
10	8.1 (2.5)	9.0 (2.8)	1.0 (0.3)	12.0 (3.8)	17.1 (5.4)	2.4 (0.8)	20.0 (6.3)	26.4 (8.3)

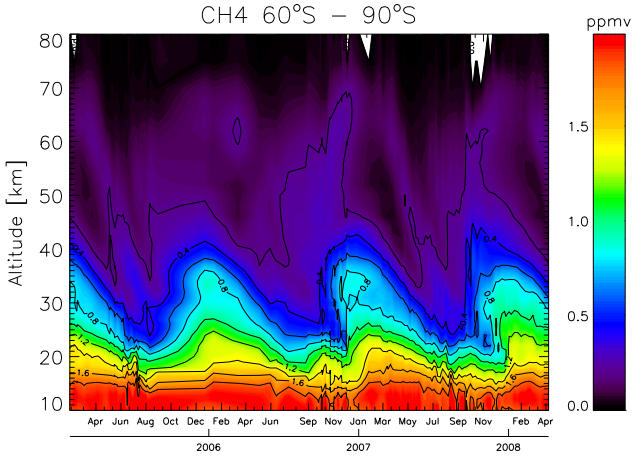

Fig. 10. Temporal development of CH_4 as a function of altitude in the southern polar region (averaged from 60° S to 90° S). White areas at high altitudes represent insignificant negative values.

subsides into the stratosphere during each of the three Southern winters. Then, after the vortex breakdown, CH_4-rich air is transported to polar latitudes in the lower stratosphere. Also in the northern polar winters subsidence occurs in each polar winters, as seen in the N_2O temporal development (Fig. 12). Rapid enhancements, are attributed to final warmings (March/April 2005–2007) or a midwinter warming (January 2006, Manney et al. 2008). At altitudes above 40 km, subsided air rich in N_2O produced in the mesosphere (Funke et al., 2008) might also have contributed to N_2O enhancements.

9 $ClONO_2$

For $ClONO_2$ the same spectral analysis window as for the original full spectral resolution retrievals (Höpfner et al., 2004a, 2007) was used, which includes the Q branch of the $ClONO_2$ ν_4 band. Absorption cross-sections by Birk and Wagner (2000) are used. Although O_3 retrievals are available from a previous retrieval step, O_3 is jointly fitted to avoid problems with misfitted lines at 779.6, 779,8, 780.15, 780.4, 780.6 and 780.8 cm^{-1} which might propagate errors to the $ClONO_2$ vmr. Compared to the original data version V2_ClONO2_1 (Höpfner et al., 2004b), later versions, e.g. the full spectral resolution data sets V3o_ClONO2_10/11 validated by Höpfner et al. (2007) and the current reduced spectral resolution data set V4o_ClONO2_201 uses a weaker regularization at higher altitudes, since the original retrieval was found to smear out $ClONO_2$ variability in the middle and

Table 11. $ClONO_2$ retrieval error budget.

Height km	Noise pptv (%)	Pointing pptv (%)	Gain pptv (%)	T pptv (%)	Precision pptv (%)	ILS pptv (%)	Spectroscopy pptv (%)	Total error pptv (%)
50	76.0 (34.7)	20.0 (9.1)	33.0 (15.1)	15.0 (6.8)	86.5 (39.5)	33.0 (15.1)	9.6 (4.4)	93.1 (42.5)
40	93.0 (18.3)	5.8 (1.1)	20.0 (3.9)	4.9 (1.0)	95.4 (18.8)	37.0 (7.3)	25.0 (4.9)	105.4 (20.7)
35	71.0 (13.3)	9.5 (1.8)	8.6 (1.6)	7.1 (1.3)	72.5 (13.6)	13.0 (2.4)	28.0 (5.2)	78.8 (14.7)
30	55.0 (8.3)	20.0 (3.0)	13.0 (2.0)	6.0 (0.9)	60.2 (9.1)	26.0 (3.9)	33.0 (5.0)	73.5 (11.1)
25	46.0 (7.2)	11.0 (1.7)	8.7 (1.4)	4.5 (0.7)	48.3 (7.5)	15.0 (2.3)	32.0 (5.0)	59.8 (9.4)
20	37.0 (7.4)	9.1 (1.8)	6.8 (1.4)	1.2 (0.2)	38.7 (7.8)	8.2 (1.6)	26.0 (5.2)	47.4 (9.5)
15	29.0 (7.8)	5.1 (1.4)	5.5 (1.5)	0.5 (0.1)	30.0 (8.0)	1.4 (0.4)	19.0 (5.1)	35.5 (9.5)
10	23.0 (50.7)	5.6 (12.4)	1.0 (2.2)	0.8 (1.8)	23.7 (52.3)	0.4 (0.9)	2.6 (5.7)	23.9 (52.6)

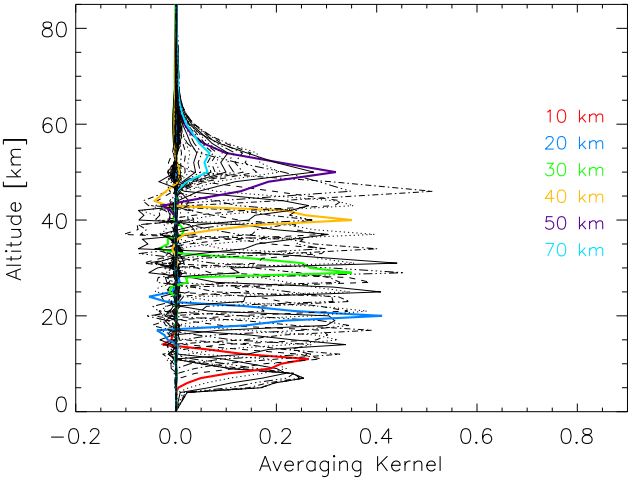

Fig. 11. Rows of the averaging kernel matrix for N_2O. For details, see Fig. 1.

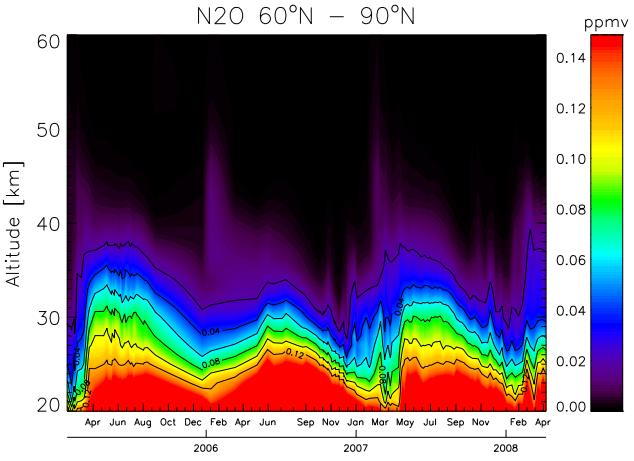

Fig. 12. Temporal development of N_2O as a function of altitude in the northern polar region (averaged from 60° N to 90° N).

upper stratosphere. The analysis window has remained unchanged (Table 1b).

The estimated retrieval error, evaluated for the limb scan recorded at 61° N, 124° W on 27 January 2005, varies between 35.5 and 105.4 pptv and is dominated by measurement noise (Table 11). The altitude resolution as inferred from the rows of the vertical averaging kernels (Fig. 13) is 2.5–3.5 km in the lowermost stratosphere, and degrades towards about 9 km at 40 km altitude (Table 2). In contrast, the altitude resolution of the full spectral resolution retrievals, version V3o_ClONO2_12 are never better than 3 km. The horizontal smoothing length of the reduced resolution nominal mode $ClONO_2$ measurements varies between 250 and 510 km for the test case under analysis (Table 3). The information displacement (Table 4) is largely dominated by the displacement of the actual tangent points. The low displacement at high altitudes reflects the effect of vertical regularization: The measurements on the uppermost tangent altitudes contain nearly no information on $ClONO_2$, and the vertical averaging kernel peaks below the nominal altitude of 50 km (cf. the violet line in Fig. 13). This vertical information shift implies also a horizontal information shift, because lower tangent points are closer to the satellite than higher ones.

Figure 14 shows a latitudinal distribution of $ClONO_2$ as a function of time. $ClONO_2$ reaches its maximum in northern polar spring. Since denitrification is stronger in the Southern polar vortex, and since ozone is largely depleted, leading to low ClO abundances, there is very little $ClONO_2$ in the core region of the vortex there. $ClONO_2$ is formed in the collar of polar vortices rather than the core region. As a consequence, at Southern polar latitudes the region of highest $ClONO_2$ mixing ratios is shifted from the pole towards midlatitudes. Wave activity moving the polar vortex off the pole masks this effect in the Northern Hemisphere.

10 ClO

For ClO the same spectral analysis windows were used as for the original full spectral resolution retrievals (Glatthor et al.,

Table 12. ClO retrieval error budget.

Height km	Noise pptv (%)	Pointing pptv (%)	Gain pptv (%)	T pptv (%)	Precision pptv (%)	ILS pptv (%)	Spectroscopy pptv (%)	Total error pptv (%)
50	420.0 (35.5)	11.0 (0.9)	17.0 (1.4)	16.0 (1.4)	420.8 (35.5)	25.0 (2.1)	130.0 (11.0)	441.1 (37.3)
40	780.0 (31.8)	9.0 (0.4)	33.0 (1.3)	23.0 (0.9)	781.1 (31.9)	42.0 (1.7)	310.0 (12.6)	841.4 (34.3)
35	610.0 (37.1)	3.1 (0.2)	21.0 (1.3)	8.8 (0.5)	610.4 (37.1)	32.0 (1.9)	280.0 (17.0)	672.3 (40.9)
30	300.0 (35.9)	6.7 (0.8)	4.9 (0.6)	1.0 (0.1)	300.1 (35.9)	14.0 (1.7)	120.0 (14.4)	323.5 (38.7)
25	290.0 (75.3)	3.4 (0.9)	1.3 (0.3)	2.4 (0.6)	290.0 (75.4)	5.2 (1.4)	60.0 (15.6)	296.2 (77.0)
20	380.0 (128.3)	28.0 (9.5)	3.4 (1.1)	3.4 (1.1)	381.1 (128.7)	3.9 (1.3)	56.0 (18.9)	385.2 (130.1)
15	200.0 (160.5)	53.0 (42.5)	13.0 (10.4)	16.0 (12.8)	207.9 (166.8)	1.0 (0.8)	47.0 (37.7)	213.2 (171.0)
10	16.0 (56.5)	8.7 (30.7)	3.0 (10.6)	2.7 (9.5)	18.7 (65.9)	0.5 (1.9)	2.5 (8.8)	18.8 (66.5)

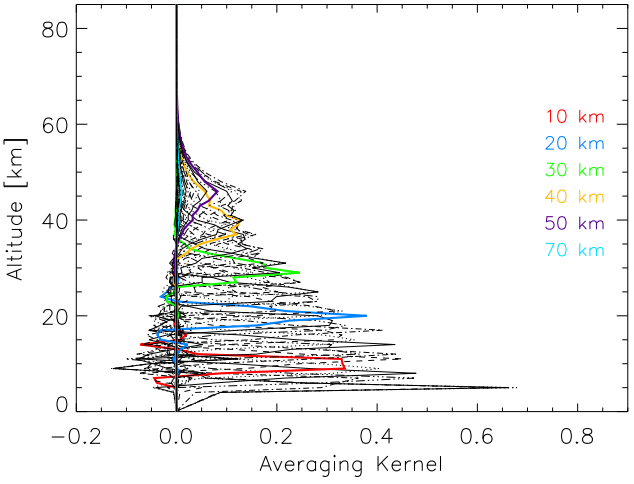

Fig. 13. Rows of the averaging kernel matrix for $ClONO_2$. For details, see Fig. 1.

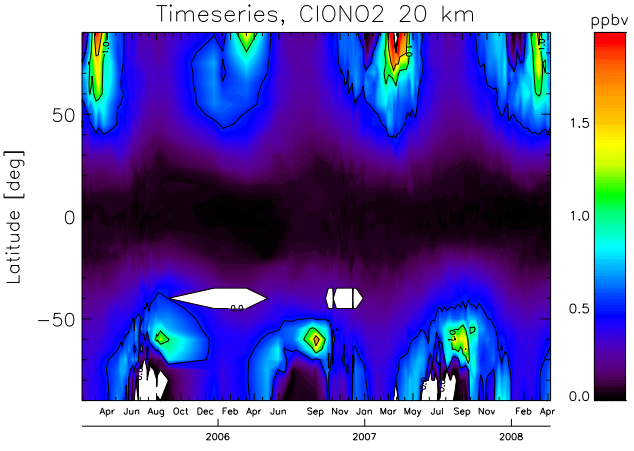

Fig. 14. Temporal development of $ClONO_2$ as a function of latitude at 20 km altitude. White areas in southern midlatitudes are due to data gaps caused by regular calibration measurements, while white areas at high southern latitudes are data gaps due to polar stratospheric clouds (PSC).

2004) (Table 1c), which includes lines in the P and Q branch region of the ClO 1–0 band. As for $ClONO_2$, O_3 is jointly fitted in order to reduce related error propagation. The same regularization as for the original data version V2_ClO_1 and more recent full spectral resolution ClO data versions up to V2_ClO_11 was used. The total retrieval error, evaluated for a limb scan recorded at 57° N, 35° W on 22 February 2007, 08:01:39 UTC, corresponding to 10:21:39 local mean time, under daytime conditions (19° solar elevation) is dominated by measurement noise. For this case of unperturbed chemical conditions, i.e. without chlorine activation, the retrieval error exceeds the 100% limit at altitudes below 20 km and is never better than 34% above (Table 12). This means that under unperturbed conditions stratospheric ClO cannot be detected in the lower stratosphere from single limb scans, and the information in the upper stratosphere is limited. However, the significance of the results can be enhanced at the cost of spatial and temporal resolution by averaging of multiple limb scans.

The altitude resolution as inferred from the rows of the vertical averaging kernels (Fig. 15) is about 3–7 km in the lower stratosphere (Table 2), and the horizontal resolution is in the order of 500 km (Table 3). The effect of horizontal information displacement at high altitudes (Table 4) is even more pronounced as for $ClONO_2$ but the same explanation applies.

Figure 16 is a latitudinal distribution of daytime ClO at 20 km as a function of time. Chlorine activation is clearly visible in Southern polar spring, and, to a lesser extent, also in northern polar late winters. Pronounced scatter and negative values at tropical latitudes reflect noisy data, since atmospheric background ClO is below the MIPAS detection limit.

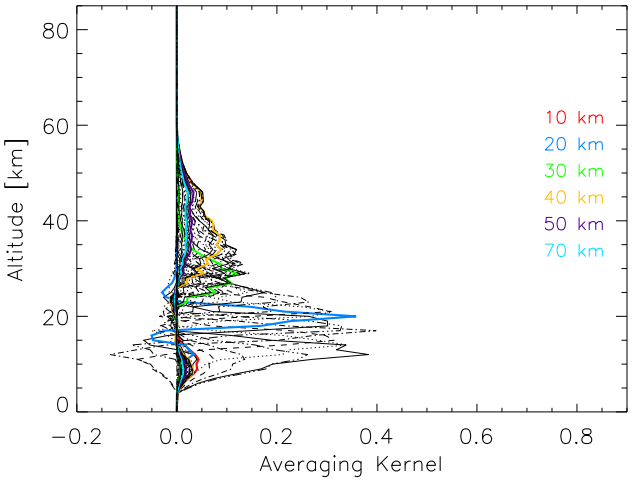

Fig. 15. Rows of the averaging kernel matrix for ClO, evaluated for a limb scan recorded at 57° N, 35° W on 22 February 2007, 08:01:39 UTC.

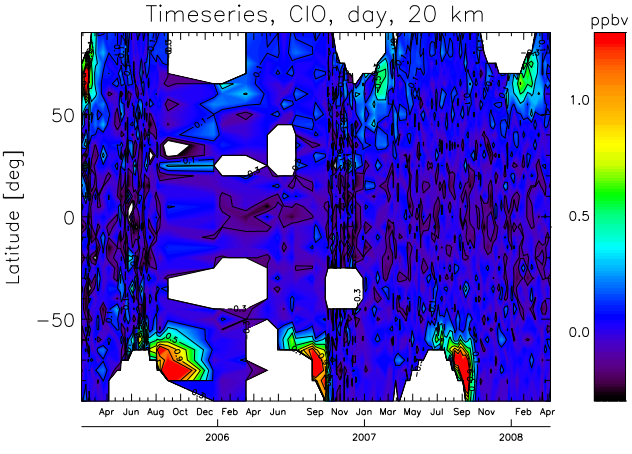

Fig. 16. Temporal development of daytime ClO as a function of latitude at 20 km altitude. White areas are data gaps caused by regular calibration measurements, due to polar stratospheric clouds (PSC), or at areas where during polar winter no daytime measurements are available.

11 Conclusions

We have presented the IMK-IAA retrievals of atmospheric state variables from MIPAS reduced resolution nominal mode measurements. The MIPAS reduced resolution nominal mode IMK-IAA retrievals are, along with related diagnostics, available to registered users via http://www.fzk.de/imk/asf/sat/envisat-data. For the species investigated in this paper, the reduction of spectral resolution seems to be rather an advantage than a drawback, because, as a consequence of denser vertical sampling of the measurements, the vertical resolution has become better. Since overlapping fields of view cause oversampling, also the retrieval error is reduced in many cases. The characteristics of data is roughly comparable to those of the reduced resolution UT/LS measurement mode retrievals (Chauhan et al., 2009), except for the horizontal smearing, which is larger for the "reduced resolution nominal mode" measurements due to the extended altitude range of the latter. In turn, due to the extension of measurements to tangent altitudes above 49 km up to 70 km, the nominal mode retrievals obviously contain more information on the upper part of the atmosphere. However, the horizontal sampling of the measurements is – similar as for the full spectral resolution measurements (von Clarmann et al., 2008) – significantly coarser than the horizontal smoothing, which implies the risk of aliasing if short scale periodic atmospheric structures are present. The inclusion of horizontal temperature gradients is important to prevent failure of convergence of many retrievals, particularly near the boundary of the polar vortex and to improve the data quality.

Acknowledgements. ESA has provided MIPAS level-1. Parts of this work has been funded by BMBF under contract no. 50 EE 0512 and by Spanish MICINN under contract AYA2008-03498/ESP and EC FEDER funds. A part of the retrievals was performed on the HP XC4000 of the Scientific Supercomputing Center (SSC) Karlsruhe under project grant MIPAS.

Edited by: M. Weber

References

Birk, M. and Wagner, G.: A New Spectroscopic Database for Chlorine Nitrate, in: Proceedings of the 6th Biennial HITRAN Database Conference, 19.–21.06.2000, Cambridge, MA, 2000.

Burgess, A. B., Grainger, R. G., Dudhia, A., Payne, V. H., and Jay, V. L.: MIPAS measurement of sulphur hexafluoride (SF_6), Geophys. Res. Lett., 31, L05112, doi:10.1029/2003GL019143, 2004.

Burgess, A. B., Grainger, R. G., and Dudhia, A.: Zonal mean atmospheric distribution of sulphur hexafluoride (SF_6), Geophys. Res. Lett., 33, L07809, doi:10.1029/2005GL025410, 2006.

Ceccherini, S., Cortesi, U., Verronen, P. T., and Kyrölä, E.: Technical Note: Continuity of MIPAS-ENVISAT operational ozone data quality from full- to reduced-spectral-resolution operation mode, Atmos. Chem. Phys., 8, 2201–2212, 2008, http://www.atmos-chem-phys.net/8/2201/2008/.

Chauhan, S., Höpfner, M., Stiller, G. P., von Clarmann, T., Funke, B., Glatthor, N., Grabowski, U., Linden, A., Kellmann, S., Milz, M., Steck, T., Fischer, H., Froidevaux, L., Lambert, A., Santee, M. L., Schwartz, M., Read, W. G., and Livesey, N. J.: MIPAS reduced spectral resolution UTLS-1 mode measurements of temperature, O_3, HNO_3, N_2O, H_2O and relative humidity over ice: retrievals and comparison to MLS, Atmos. Meas. Tech. Discuss., 2, 439–487, 2009, http://www.atmos-meas-tech-discuss.net/2/439/2009/.

Echle, G., von Clarmann, T., Dudhia, A., Flaud, J.-M., Funke, B., Glatthor, N., Kerridge, B., López-Puertas, M., Martín-Torres, F. J., and Stiller, G. P.: Optimized spectral microwindows for data analysis of the Michelson Interferometer for Passive Atmospheric Sounding on the Environmental Satellite, Appl. Optics, 39, 5531–5540, 2000.

Fischer, H., Birk, M., Blom, C., Carli, B., Carlotti, M., von Clarmann, T., Delbouille, L., Dudhia, A., Ehhalt, D., Endemann, M., Flaud, J. M., Gessner, R., Kleinert, A., Koopman, R., Langen, J., López-Puertas, M., Mosner, P., Nett, H., Oelhaf, H., Perron, G., Remedios, J., Ridolfi, M., Stiller, G., and Zander, R.: MIPAS: an instrument for atmospheric and climate research, Atmos. Chem. Phys., 8, 2151–2188, 2008, http://www.atmos-chem-phys.net/8/2151/2008/.

Flaud, J.-M., Brizzi, G., Carlotti, M., Perrin, A., and Ridolfi, M.: MIPAS database: Validation of HNO_3 line parameters using MIPAS satellite measurements, Atmos. Chem. Phys., 6, 5037–5048, 2006, http://www.atmos-chem-phys.net/6/5037/2006/.

Funke, B., López-Puertas, M., Stiller, G. P., von Clarmann, T., and Höpfner, M.: A new non–LTE Retrieval Method for Atmospheric Parameters From MIPAS–ENVISAT Emission Spectra, Adv. Space Res., 27, 1099–1104, 2001.

Funke, B., López-Puertas, M., von Clarmann, T., Stiller, G. P., Fischer, H., Glatthor, N., Grabowski, U., Höpfner, M., Kellmann, S., Kiefer, M., Linden, A., Mengistu Tsidu, G., Milz, M., Steck, T., and Wang, D. Y.: Retrieval of stratospheric NO_x from 5.3 and 6.2 μm nonlocal thermodynamic equilibrium emissions measured by Michelson Interferometer for Passive Atmospheric Sounding (MIPAS) on Envisat, J. Geophys. Res., 110, D09302, doi:10.1029/2004JD005225, 2005.

Funke, B., López-Puertas, M., Garcia-Comas, M., Stiller, G. P., von Clarmann, T., and Glatthor, N.: Mesospheric N_2O enhancements as observed by MIPAS on Envisat during the polar winters in 2002–2004, Atmos. Chem. Phys., 8, 5787–5800, 2008, http://www.atmos-chem-phys.net/8/5787/2008/.

Glatthor, N., von Clarmann, T., Fischer, H., Grabowski, U., Höpfner, M., Kellmann, S., Kiefer, M., Linden, A., Milz, M., Steck, T., Stiller, G. P., Mengistu Tsidu, G., Wang, D. Y., and Funke, B.: Spaceborne ClO observations by the Michelson Interferometer for Passive Atmospheric Sounding (MIPAS) before and during the Antarctic major warming in September/October 2002, J. Geophys. Res., 109, D11307, doi:10.1029/2003JD004440, 2004.

Glatthor, N., von Clarmann, T., Fischer, H., Funke, B., Grabowski, U., Höpfner, M., Kellmann, S., Kiefer, M., Linden, A., Milz, M., Steck, T., Stiller, G. P., Mengistu Tsidu, G., and Wang, D. Y.: Mixing processes during the Antarctic vortex split in September/October 2002 as inferred from source gas and ozone distributions from ENVISAT-MIPAS, J. Atmos. Sci., 62, 787–800, 2005.

Glatthor, N., von Clarmann, T., Fischer, H., Funke, B., Gil-López, S., Grabowski, U., Höpfner, M., Kellmann, S., Linden, A., López-Puertas, M., Mengistu Tsidu, G., Milz, M., Steck, T., Stiller, G. P., and Wang, D.-Y.: Retrieval of stratospheric ozone profiles from MIPAS/ENVISAT limb emission spectra: a sensitivity study, Atmos. Chem. Phys., 6, 2767–2781, 2006, http://www.atmos-chem-phys.net/6/2767/2006/.

Hoffmann, L., Kaufmann, M., Spang, R., Müller, R., Remedios, J. J., Moore, D. P., Volk, C. M., von Clarmann, T., and Riese, M.: Envisat MIPAS measurements of CFC-11: retrieval, validation, and climatology, Atmos. Chem. Phys., 8, 3671–3688, 2008, http://www.atmos-chem-phys.net/8/3671/2008/.

Höpfner, M., von Clarmann, T., Fischer, H., Glatthor, N., Grabowski, U., Kellmann, S., Kiefer, M., Linden, A., Mengistu Tsidu, G., Milz, M., Steck, T., Stiller, G. P., Wang, D.-Y., and Funke, B.: First spaceborne observations of Antarctic stratospheric $ClONO_2$ recovery: Austral spring 2002, J. Geophys. Res., 109, D11308, doi:10.1029/2004JD004609, 2004a.

Höpfner, M., von Clarmann, T., Fischer, H., Glatthor, N., Grabowski, U., Kellmann, S., Kiefer, M., Linden, A., Mengistu Tsidu, G., Milz, M., Steck, T., Stiller, G. P., Wang, D.-Y., and Funke, B.: First spaceborne observations of Antarctic stratospheric $ClONO_2$ recovery: Austral spring 2002, J. Geophys. Res., 109, D11308, doi:10.1029/2004JD004609, 2004b.

Höpfner, M., von Clarmann, T., Fischer, H., Funke, B., Glatthor, N., Grabowski, U., Kellmann, S., Kiefer, M., Linden, A., Milz, M., Steck, T., Stiller, G. P., Bernath, P., Blom, C. E., Blumenstock, Th., Boone, C., Chance, K., Coffey, M. T., Friedl-Vallon, F., Griffith, D., Hannigan, J. W., Hase, F., Jones, N., Jucks, K. W., Keim, C., Kleinert, A., Kouker, W., Liu, G. Y., Mahieu, E., Mellqvist, J., Mikuteit, S., Notholt, J., Oelhaf, H., Piesch, C., Reddmann, T., Ruhnke, R., Schneider, M., Strandberg, A., Toon, G., Walker, K. A., Warneke, T., Wetzel, G., Wood, S., and Zander, R.: Validation of MIPAS $ClONO_2$ measurements, Atmos. Chem. Phys., 7, 257–281, 2007, http://www.atmos-chem-phys.net/7/257/2007/.

Manney, G. L., Krueger, K., Pawson, S., Minschwaner, K., Schwartz, M. J., Daffer, W., Livesey, N. J., Mlynczak, M. G., Remsberg, E., Russell, J. M., and Waters, J. W.: The evolution of the stratopause during the 2006 major warming: Satellite Data and Assimilated Meteorological Analyses, J. Geophys. Res., 113, D11115 doi:10.1029/2007JD009097, 2008.

Mengistu Tsidu, G., Stiller, G. P., von Clarmann, T., Funke, B., Höpfner, M., Fischer, H., Glatthor, N., Grabowski, U., Kellmann, S., Kiefer, M., Linden, A., López-Puertas, M., Milz, M., Steck, T., and Wang, D. Y.: NO_y from Michelson Interferometer for Passive Atmospheric Sounding on Environmental Satellite during the Southern Hemisphere polar vortex split in September/October 2002, J. Geophys. Res., 110, D11301, doi:10.1029/2004JD005322, 2005.

Milz, M., von Clarmann, T., Fischer, H., Glatthor, N., Grabowski, U., Höpfner, M., Kellmann, S., Kiefer, M., Linden, A., Mengistu Tsidu, G., Steck, T., Stiller, G. P., Funke, B., López-Puertas, M., and Koukouli, M. E.: Water Vapor Distributions Measured with the Michelson Interferometer for Passive Atmospheric Sounding on board Envisat (MIPAS/Envisat), J. Geophys. Res., 110, D24307, doi:10.1029/2005JD005973, 2005.

Milz, M., Clarmann, T. v., Bernath, P., Boone, C., Buehler, S. A., Chauhan, S., Deuber, B., Feist, D. G., Funke, B., Glatthor, N., Grabowski, U., Griesfeller, A., Haefele, A., Höpfner, M., Kämpfer, N., Kellmann, S., Linden, A., Müller, S., Nakajima, H., Oelhaf, H., Remsberg, E., Rohs, S., Russell III, J. M., Schiller, C., Stiller, G. P., Sugita, T., Tanaka, T., Vömel, H., Walker, K., Wetzel, G., Yokota, T., Yushkov, V., and Zhang, G.: Validation of water vapour profiles (version 13) retrieved by the IMK/IAA scientific retrieval processor based on full resolution spectra measured by MIPAS on board Envisat, Atmos. Meas. Tech. Discuss., 2, 489–559, 2009, http://www.atmos-meas-tech-discuss.net/2/489/2009/.

Norton, H. and Beer, R.: New apodizing functions for Fourier spectrometry, J. Opt. Soc. Am, 66, 259–264, (Errata J. Opt. Soc. Am., 67, 419, 1977), 1976.

Raspollini, P., Belotti, C., Burgess, A., Carli, B., Carlotti, M., Ceccherini, S., Dinelli, B. M., Dudhia, A., Flaud, J.-M., Funke, B.,

Hpfner, M., López-Puertas, M., Payne, V., Piccolo, C., Remedios, J. J., Ridolfi, M., and Spang, R.: MIPAS level 2 operational analysis, Atmos. Chem. Phys., 6, 5605–5630, 2006, http://www.atmos-chem-phys.net/6/5605/2006/.

Remedios, J. J., Leigh, R. J., Waterfall, A. M., Moore, D. P., Sembhi, H., Parkes, I., Greenhough, J., Chipperfield, M. P., and Hauglustaine, D.: MIPAS reference atmospheres and comparisons to V4.61/V4.62 MIPAS level 2 geophysical data sets, Atmos. Chem. Phys. Discuss., 7, 9973–10017, 2007, http://www.atmos-chem-phys-discuss.net/7/9973/2007/.

Ridolfi, M., Carli, B., Carlotti, M., von Clarmann, T., Dinelli, B., Dudhia, A., Flaud, J.-M., Höpfner, M., Morris, P. E., Raspollini, P., Stiller, G., and Wells, R. J.: Optimized Forward and Retrieval Scheme for MIPAS Near-Real-Time Data Processing, Appl. Optics, 39, 1323–1340, 2000.

Rodgers, C. D.: Inverse Methods for Atmospheric Sounding: Theory and Practice, in: Series on Atmospheric, Oceanic and Planetary Physics, Vol. 2, edited by: Taylor, F. W., World Scientific, 2000.

Rothman, L. S., Barbe, A., Benner, D. C., Brown, L. R., Camy-Peyret, C., Carleer, M. R., Chance, K., Clerbaux, C., Dana, V., Devi, V. M., Fayt, A., Flaud, J.-M., Gamche, R. R., Goldman, A., Jacquemart, D., Jucks, K. W., Lafferty, W. J., Mandin, J.-Y., Massie, S. T., Nemtchinov, V., Newnham, D. A., Perrin, A., Rinsland, C. P., Schroeder, J., Smith, K. M., Smith, M. A. H., Tang, K., Toth, R. A., Vander Auwera, J., Varanasi, P., and Yoshino, K.: The HITRAN molecular spectroscopic database: edition of 2000 including updates through 2001, J. Quant. Spectrosc. Radiat. Transfer, 82, 5–44, doi:10.1016/S0022-4073(03)00146-8, 2003.

Steck, T.: Methods for determining regularization for atmospheric retrieval problems, Appl. Optics, 41, 1788–1797, 2002.

Steck, T. and von Clarmann, T.: Constrained profile retrieval applied to the observation mode of the Michelson Interferometer for Passive Atmospheric Sounding, Appl. Optics, 40, 3559–3571, 2001.

Steck, T., von Clarmann, T., Fischer, H., Funke, B., Glatthor, N., Grabowski, U., Höpfner, M., Kellmann, S., Kiefer, M., Linden, A., Milz, M., Stiller, G. P., Wang, D. Y., Allaart, M., Blumenstock, Th., von der Gathen, P., Hansen, G., Hase, F., Hochschild, G., Kopp, G., Kyrö, E., Oelhaf, H., Raffalski, U., Redondas Marrero, A., Remsberg, E., Russell III, J., Stebel, K., Steinbrecht, W., Wetzel, G., Yela, M., and Zhang, G.: Bias determination and precision validation of ozone profiles from MIPAS-Envisat retrieved with the IMK-IAA processor, Atmos. Chem. Phys., 7, 3639–3662, 2007, http://www.atmos-chem-phys.net/7/3639/2007/.

Tikhonov, A.: On the solution of incorrectly stated problems and method of regularization, Dokl. Akad. Nauk. SSSR, 151, 501–504, 1963.

von Clarmann, T. and Echle, G.: Selection of optimized microwindows for atmospheric spectroscopy, Appl. Optics, 37, 7661–7669, 1998.

von Clarmann, T., Glatthor, N., Grabowski, U., Höpfner, M., Kellmann, S., Kiefer, M., Linden, A., Mengistu Tsidu, G., Milz, M., Steck, T., Stiller, G. P., Wang, D. Y., Fischer, H., Funke, B., Gil-López, S., and López-Puertas, M.: Retrieval of temperature and tangent altitude pointing from limb emission spectra recorded from space by the Michelson Interferometer for Passive Atmospheric Sounding (MIPAS), J. Geophys. Res., 108, 4736, doi:10.1029/2003JD003602, 2003.

von Clarmann, T., De Clercq, C., Ridolfi, M., Hpfner, M., and Lambert, J.-C.: The horizontal resolution of MIPAS, Atmos. Meas. Tech. Discuss., 1, 103–125, 2008, http://www.atmos-meas-tech-discuss.net/1/103/2008/.

Wang, D. Y., von Clarmann, T., Fischer, H., Funke, B., Gil-López, S., Glatthor, N., Grabowski, U., Höpfner, M., Kaufmann, M., Kellmann, S., Kiefer, M., Koukouli, M. E., Linden, A., López-Puertas, M., Mengistu Tsidu, G., Milz, M., Steck, T., Stiller, G. P., Simmons, A. J., Dethof, A., Swinbank, R., Marquardt, C., Jiang, J. H., Romans, L. J., Wickert, J., Schmidt, T., Russell III, J., and Remsberg, E.: Validation of stratospheric temperatures measured by Michelson Interferometer for Passive Atmospheric Sounding MIPAS on Envisat, J. Geophys. Res., 110, D08301, doi:10.1029/2004JD005342, 2005.

Wang, D. Y., Höpfner, M., Mengistu Tsidu, G., Stiller, G. P., von Clarmann, T., Fischer, H., Blumenstock, T., Glatthor, N., Grabowski, U., Hase, F., Kellmann, S., Linden, A., Milz, M., Oelhaf, H., Schneider, M., Steck, T., Wetzel, G., López-Puertas, M., Funke, B., Koukouli, M. E., Nakajima, H., Sugita, T., Irie, H., Urban, J., Murtagh, D., Santee, M. L., Toon, G., Gunson, M. R., Irion, F. W., Boone, C. D., Walker, K., and Bernath, P. F.: Validation of nitric acid retrieved by the IMK-IAA processor from MIPAS/ENVISAT measurements, Atmos. Chem. Phys., 7, 721–738, 2007, http://www.atmos-chem-phys.net/7/721/2007/.